

Supporting Information

Gradient solid electrolyte interphase strategy through corrosion suppression and controlled crystal growth for zinc-metal batteries

Jiayu Zhang^a, Qibin Lai^a, Yihan Song^a, Jiayun Zhong^a, Xin Ji^a, Ye Liu^a, Lu Li^a, Ning Xia^a, Rong Li^a, Guoduo Yang^a, Yanfei Li^b, Haizhu Sun^{a*}

^aCollege of Chemistry, National & Local United Engineering Laboratory for Power Batteries, Northeast Normal University, No. 5268, Renmin Street, Changchun, 130024, P. R. China.

E-mail: sunhz335@nenu.edu.cn

^bState Key Laboratory of Organic Electronics and Information Displays & Institute of Advanced Materials (IAM), School of Chemistry and Life Sciences Nanjing University of Posts & Telecommunications (NJUPT), Nanjing 210023, P. R. China

Experimental section.

Material

Zinc sulfate heptahydrate ($\text{ZnSO}_4 \cdot 7\text{H}_2\text{O}$, 99.0%), glycine (AR, 99.5%), Manganese sulfate monohydrate ($\text{MnSO}_4 \cdot \text{H}_2\text{O}$, 99%), KMnO_4 (99.5%) and Sulfuric acid were purchased from Aladdin reagent Co., Ltd.

Configuration of electrolyte

The 2 M ZnSO_4 aqueous electrolyte was prepared using $\text{ZnSO}_4 \cdot 7\text{H}_2\text{O}$ and deionized water based on the molar ratio. Different amounts (0.1 mg ml^{-1} , 0.2 mg ml^{-1} , 0.3 mg ml^{-1} , 0.4 mg ml^{-1} , 0.5 mg ml^{-1}) glycine were added to 2 M ZnSO_4 electrolyte to prepare glycine electrolytes at different concentrations. This electrolyte is used in half-cells. For full batteries, it should be noted that an additional concentration of 0.1 M $\text{MnSO}_4 \cdot \text{H}_2\text{O}$.

Synthesis of MnO_2 cathode

3 mmol of $\text{MnSO}_4 \cdot \text{H}_2\text{O}$ and 2 mL of $0.5 \text{ mol L}^{-1} \text{H}_2\text{SO}_4$ were added to 60 mL of distilled water and stirred magnetically for 30 min, then 20 mL of $0.1 \text{ mol L}^{-1} \text{KMnO}_4$ was slowly added to the above solution, stirred for 1 h and ultrasonicated for 1 h at room temperature, and then the resultant solution was transferred to a sealed PTFE lined autoclave and reacted at $120 \text{ }^\circ\text{C}$ for 12 h. After cooling to room temperature, the reaction was washed with distilled water. Finally, freeze-drying was performed to successfully produce MnO_2 .

Characterization.

The X-ray diffraction (XRD) patterns were collected on a Dmax2200PC with Cu K α radiation. The morphologies of the zinc metal were confirmed by scanning electron microscope (SEM, HITACHI SU8010). The composition and surface oxidation state of different Zn metal electrodes were probed by X-ray photoelectron spectroscopy (XPS) by using SHIMADZU AXIS SUPRA+ with Al K-Alpha X-ray as the excitation source. The solvation structures of Zn^{2+} in various solutions were studied by Fourier-transform infrared spectroscopy (FTIR), Raman microscope and liquid-state nuclear magnetic resonance (NMR). NMR were collected by Avance NEO 500. Raman spectra

were performed by an LabRAM Odyssey to obtain Raman signals of the electrolytes. FTIR spectroscopy was performed on NICOLET iS50. The charge transfer resistance and ionic conductivities of the electrolytes were recorded using the CHI660. The optical images of zinc anode were observed by Phenix Industrial Digital Camera MC-D600U3(C)Pro. Assemble a zinc-zinc symmetric open cell using a cuvette. A digital camera was used to take in situ photographs of the electrode surface during deposition.

Electrochemical Measurements.

The active material (MnO_2), the conductive material (Super P), and the binder (polyvinylidene fluoride, PVDF) were ground and mixed in a mass ratio of 7:2:1, and then an appropriate amount of N-methyl-2-pyrrolidone (NMP) was added to prepare the slurry. The prepared slurry was uniformly applied to the carbon paper collector and then dried in a blast drying oven at 60 °C for more than 12 hours. The mass loading of the prepared MnO_2 electrodes was 1 mg cm^{-2} . Zn metal plates (100 μm) were cut into suitable discs for direct use as electrodes for symmetrical, asymmetrical and standard full batteries, and glass fibers (Waterman, 19 mm in diameter) were used as diaphragms for the cells. A coin cell (type 2032) was selected for electrochemical tests with an electrolyte volume of 100 μL and the volume of 2 M ZnSO_4 or 0.1M MnSO_4 +2 M ZnSO_4 /glycine for pouch cell was 1.0 mL. The electrochemical performance of Zn// MnO_2 cells was tested in the voltage range of 0.8-1.9 V.

The electrochemical impedance spectra (EIS) were recorded at open circuit voltages from 100 KHz to 10 mHz. All electrochemical tests were performed on a Neware battery tester. Zn//Zn symmetric cells were constructed to test the reversibility of Zn plating/stripping at different current densities (0.5-10 mA cm^{-2}) and deposition capacities (0.5-10 mAh cm^{-2}). Zn//Cu half cells were tested to get the Coulombic efficiencies (CE) of Zn plating/stripping. The traditional CE test was performed by plating a quantity of Zn (4/5 mA cm^{-2} , 1 mAh cm^{-2}) on a copper electrode and charging it to 0.4 V. The amount of Zn that can be stripped per cycle was divided by the amount of Zn deposited to obtain the value of CEs. In addition, in order to more accurately assess the effect of the glycine additive on CE, a "pre-activation mode" method was also chosen to test the CE value. In this mode, a Zn reservoir was created by plating 5 mAh cm^{-2} of Zn on Cu foil and then charging to 0.4 V to strip active Zn. Linear sweep voltammetry (LSV) and other some

electrochemical characterizations (such as Cyclic voltammetry (CV)) were measured with the electrochemical workstation (CHI660).

Calculation details.

All calculations were performed using the Vienna Ab Initio Simulation Package (VASP), based on density functional theory (DFT). Core-valence interactions were described using the Projector Augmented Wave (PAW) method, and the local density was approximated with the Generalized Gradient Approximation (GGA) based on the PBE exchange-correlation functional. The Brillouin zone was sampled using the Monkhorst-Pack method. A plane-wave cutoff energy (ENCUT) of 400 eV was used, with K points optimized for convergence, ranging from $1\times 1\times 1$ to $3\times 3\times 1$. Convergence criteria for electron and ion relaxation were set to 1.0×10^{-4} eV and 1.0×10^{-3} eV, respectively, while the force convergence criterion was 0.02 eV/Å.

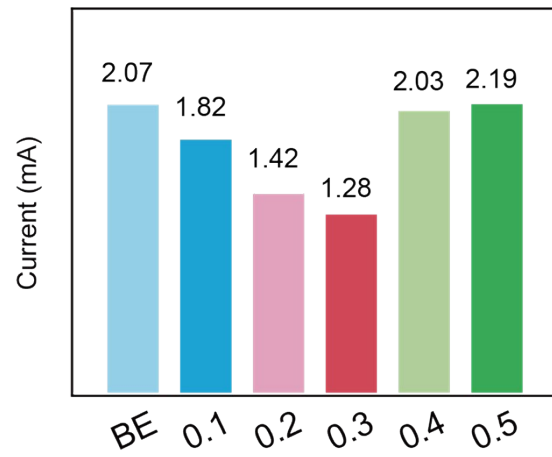


Fig. S1 Corrosion currents of different electrolytes.

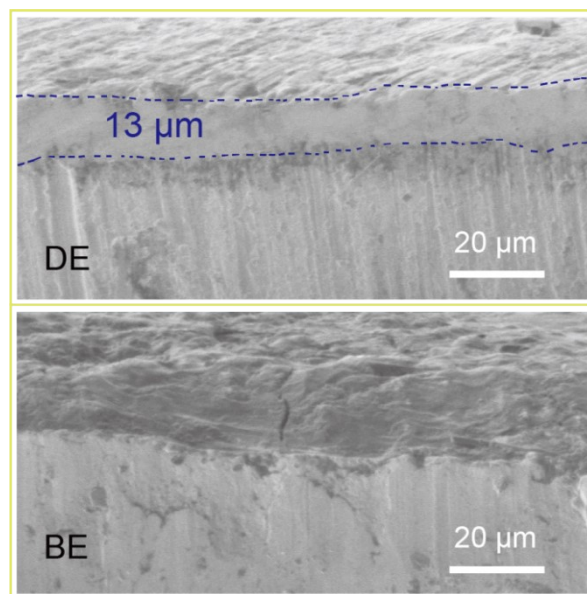


Fig. S2 SEM images of Zn anode after 20 cycles in BE and DE electrolyte.

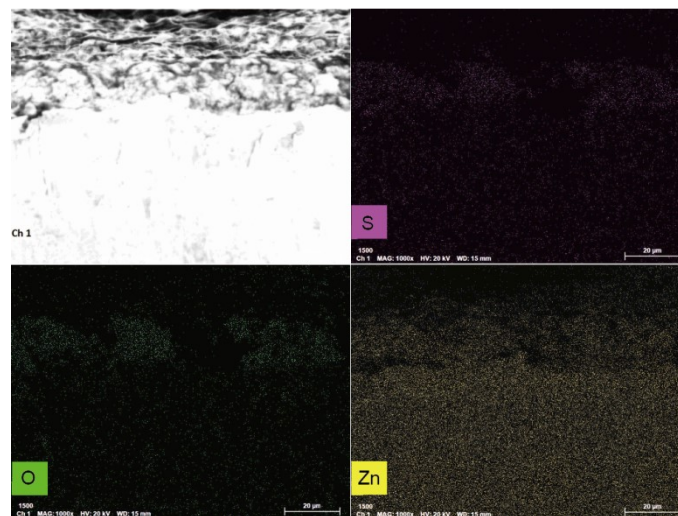


Fig. S3 Element mapping images of Zn anode after 20 cycles in DE electrolyte.

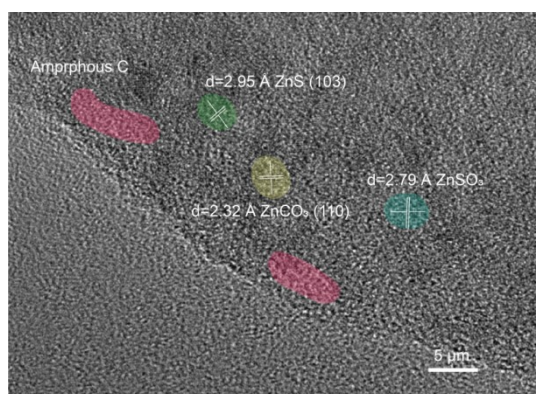


Fig. S4 High resolution transmission electron microscope image of the gradient SEI.

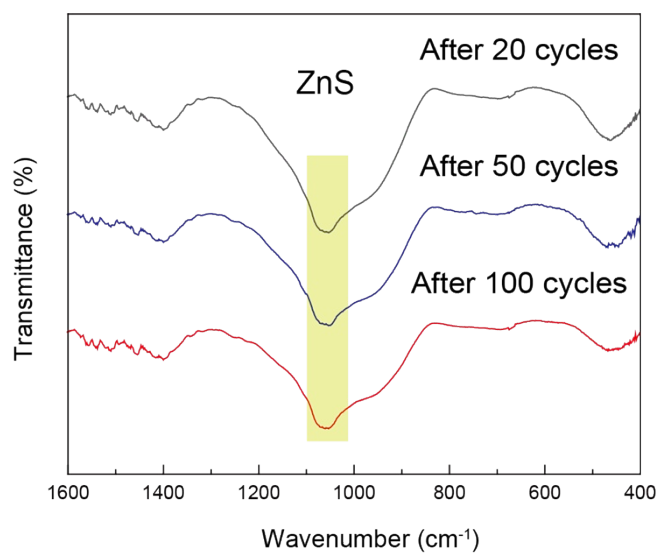


Fig. S5 FT-IR spectrum of Zn anode after different cycles in DE electrolyte.

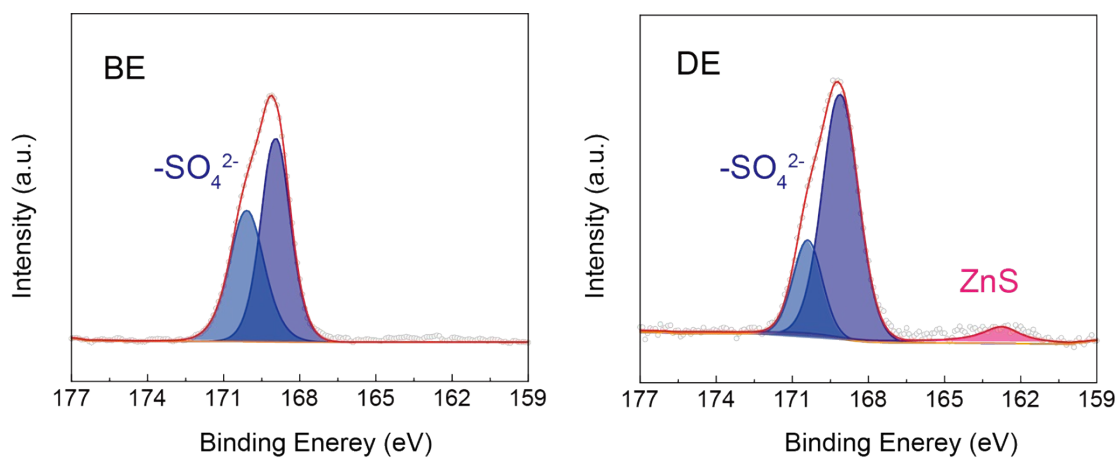


Fig. S6 XPS spectrum of Zn anode after 20 cycles in BE and DE electrolyte.

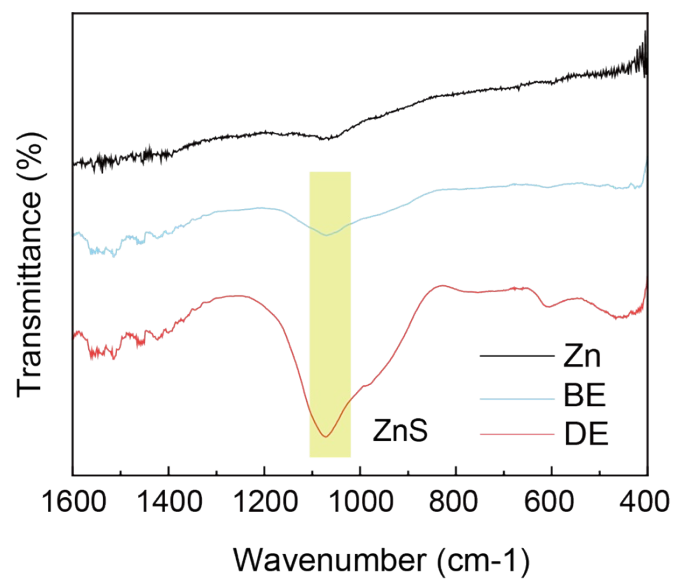


Fig. S7 FT-IR spectrum of Zn anode after 20 cycles in BE and DE electrolyte.

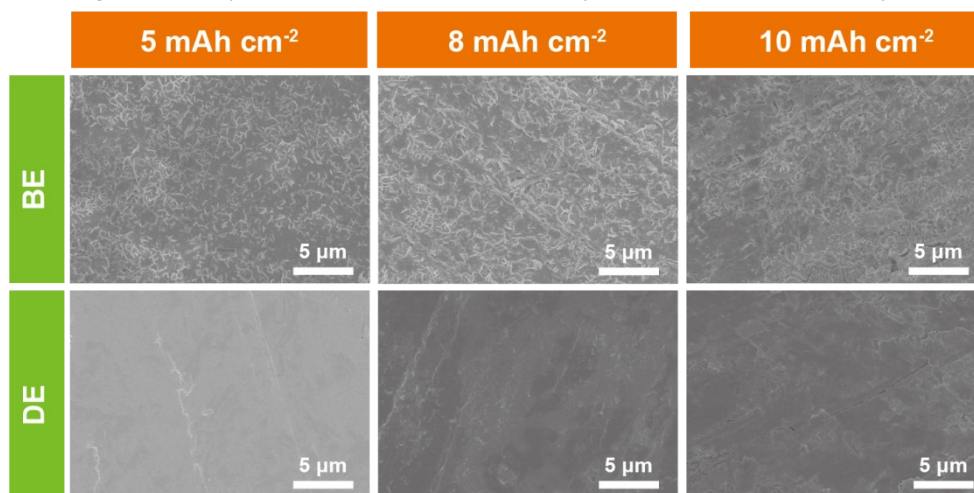


Fig. S8 SEM image for different amount of Zn deposition on anode in BE and DE electrolytes.

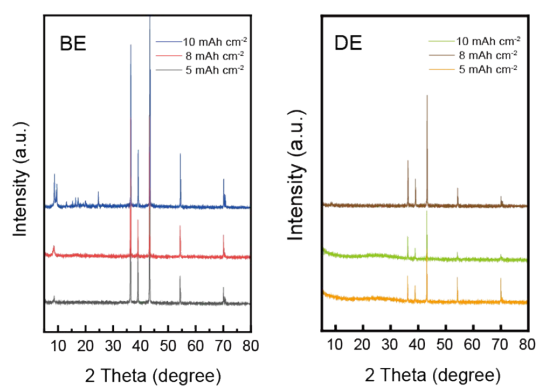


Fig. S9 XRD spectrum of Zn anode after Zn deposition in BE and DE electrolyte.

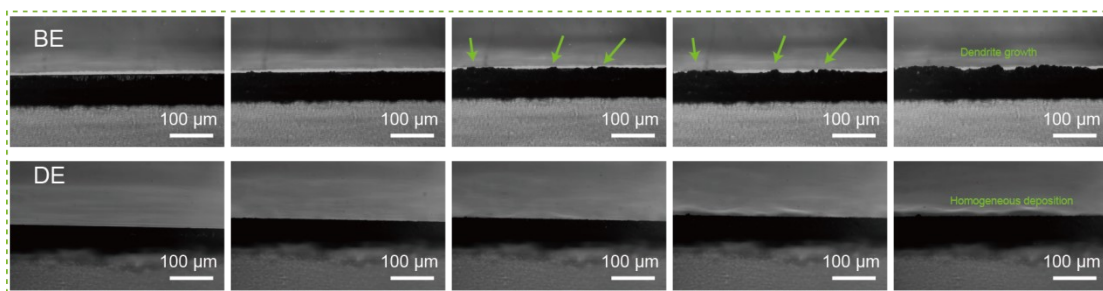


Fig. S10 In situ optical microscopy images of Zn plating behaviors in Zn//Zn cells in BE and DE electrolyte.

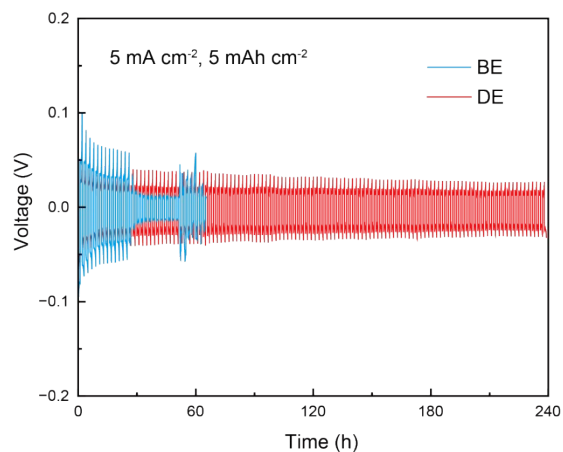


Fig. S11 Long-cycle performance testing in different electrolytes at a capacity of 5 mAh cm⁻² and a current density of 5 mA cm⁻².

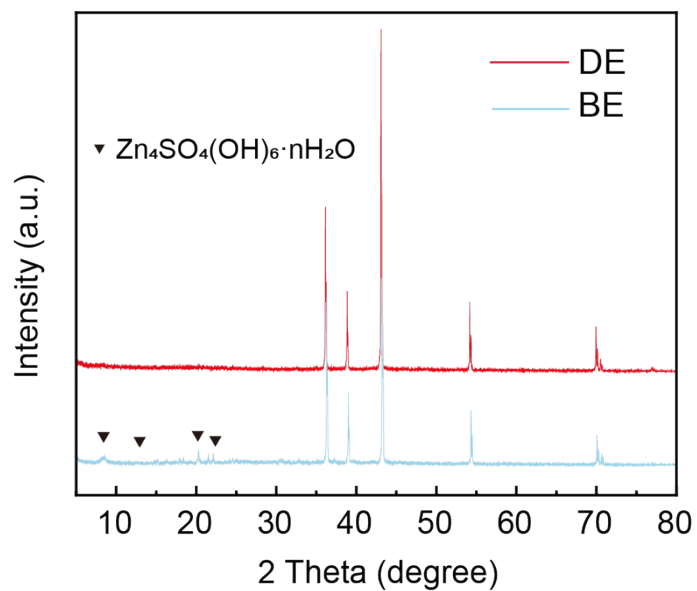


Fig. S12 XRD spectrum of Zn anode after 20 cycles in BE and DE electrolyte.

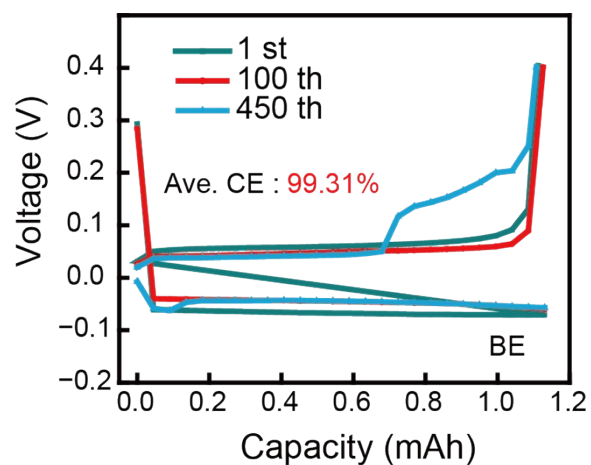


Fig. S13 Voltage – time profiles at 5 mA cm^{-2} with an areal capacity of 1 mAh cm^{-2} of the Zn//Cu cells with BE electrolyte.

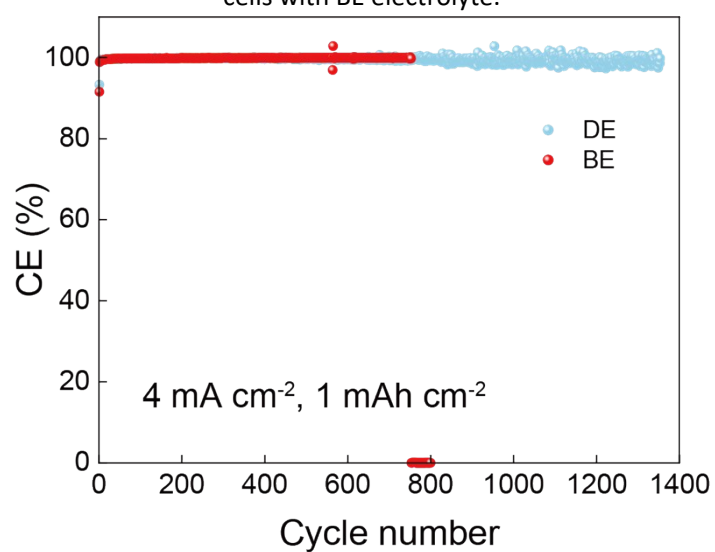


Fig. S14 CE test of Zn//Cu using BE or DE as the electrolyte at 4 mA cm^{-2} for 1 mAh cm^{-2} .

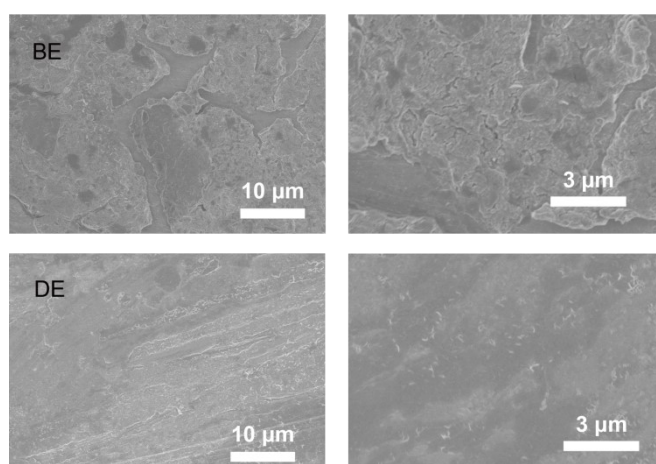


Fig. S15 SEM images of Zn flake after immersing in BE or DE electrolyte for 3 days.

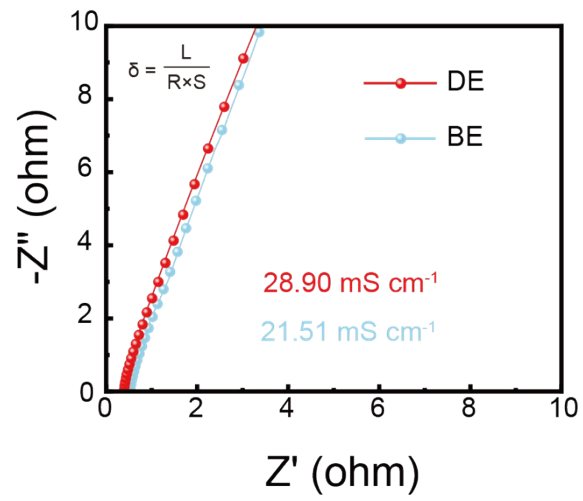


Fig. S16 Ionic conductivity test for BE and DE electrolyte.

Table S1 Comparison of the electrochemical performance Zn//Cu battery with BE and DE electrolyte.

Electrolyte composition	Current density (mA cm ⁻²)	Capacity density (mAh cm ⁻²)	Coulombic efficiency (%)	Cycle number	Ref.
2 M ZnSO ₄ /L-Cys	2	1	98.6	120	S1
2 M ZnSO ₄ /Cysteine	1	1	99.2	300	S2
2 M ZnSO ₄ /Ala ⁺	4	1	99.4	830	S3
2 M ZnSO ₄ /PGA	1	1	99.5	1200	S4
2 M ZnSO ₄ /[EMIM]OTF	1	0.5	99.6	2500	S5
2 M ZnSO ₄ /TCB	2	1	99.5	1500	S6
2 M ZnSO ₄ /NTE	5	2	99.7	300	S7
2 M ZnSO₄/Glycine	5	1	99.91	3800	This work

References:

1. W. Song, X. Xie, L. Deng, A. Pan, G. Cao, S. Liang and G. Fang, *Energy Storage Mater.*, 2024, **70**, 103489.
2. P. Jiang, Q. Du, M. Shi, W. Yang and X. Liang, *Small Methods*, 2024, **8**, 2300823.
3. G. Guo, C. Ji, J. Lin, T. Wu, Y. Luo, C. Sun, M. Li, H. Mi, L. Sun and H. J. Seifert, *Angew. Chem.-Int. Edit.*, 2024, **63**, e202407417.
4. C. Huang, J. Mao, S. Li, W. Zhang, X. Wang, Z. Shen, S. Zhang, J. Guo, Y. Xu, Y. Lu and J. Lu, *Adv. Funct. Mater.*, 2024, **34**, 2315855.
5. J. Weng, W. Zhu, K. Yu, J. Luo, M. Chen, L. Li, Y. Zhuang, K. Xia, Z. Lu, Y. Hu, C. Yang, M. Wu and Z. Zou, *Adv. Funct. Mater.*, 2024, **34**, 2314347.
6. M. Zhao, Y. Lv, J. Qi, Y. Zhang, Y. Du, Q. Yang, Y. Xu, J. Qiu, J. Lu and S. Chen, *Adv. Mater.*, 2024, **36**, 2412667.
7. K. Wang, T. Qiu, L. Lin, H. Zhan, X.-X. Liu and X. Sun, *Energy Storage Mater.*, 2024, **70**, 103516.